ACS Photonics

Letter

Cite This: ACS Photonics 2019, 6, 1602−1609

pubs.acs.org/journal/apchd5

Macroscopically Aligned Carbon Nanotubes as a Refractory Platform for Hyperbolic Thermal Emitters

Weilu Gao,[†,§] Chloe F. Doiron,[†,§] Xinwei Li,[†] Junichiro Kono,[†,‡,∥] and Gururaj V. Naik*[,†]

[†]Department of Electrical and Computer Engineering, [‡]Department of Physics and Astronomy, and [∥]Department of Materials Science and NanoEngineering, Rice University, Houston, Texas 77005, United States

Supporting Information

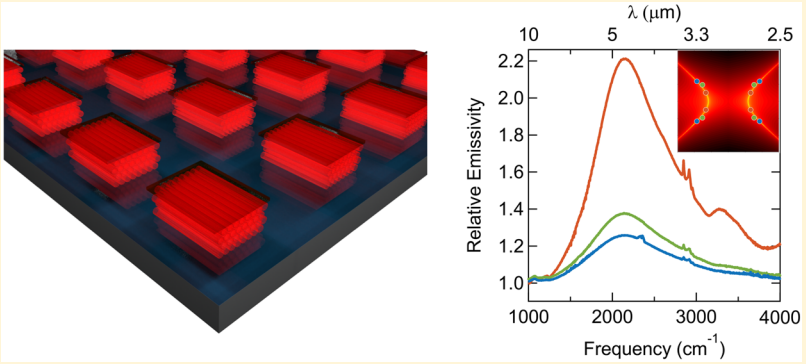

ABSTRACT: Nanophotonic thermal emitters with large photonic density of states (PDOS) have the potential to significantly enhance the efficiency of radiative cooling and waste heat recovery. Because of their nearly infinite PDOS, refractory hyperbolic materials make a promising material platform for thermal emitters. However, it is challenging to achieve a prominent PDOS in existing refractory hyperbolic materials, especially in a broad bandwidth. Here, we demonstrate macroscopically aligned carbon nanotubes as an excellent refractory material platform for hyperbolic nanophotonic devices. Aligned carbon nanotubes are thermally stable up to 1600 °C and exhibit extreme anisotropy: metallic in one direction and insulating in the other two directions. Such extreme anisotropy results in an exceptionally large PDOS over a broadband spectrum range (longer than 4.3 μm) in the mid-infrared, manifesting as strong resonances in deeply subwavelength-sized cavities. We demonstrate polarized, spectrally selective, thermal emission from aligned carbon nanotube films and indefinite cavities of volume as small as $\sim\lambda^3/700$ operating at 700 °C. These experiments suggest that aligned carbon nanotubes enhance PDOS and hence also thermal photon density by over 2 orders of magnitude, making them a promising refractory nanophotonics platform.

KEYWORDS: *aligned carbon nanotubes, refractory nanophotonics, hyperbolic materials, thermal emitters, mid-infrared*

Refractory nanophotonics, or nanophotonics at high temperatures, can revolutionize many applications, including novel infrared sources,[1−7] ultrahigh density data storage,[8,9] innovative chemical sensing techniques,[10,11] and waste heat recovery.[12−15] For example, thermophotovoltaic energy conversion, useful for waste heat recovery, can be significantly more efficient with mid-infrared refractory nanophotonic devices.[12−15] Given that waste heat accounts for 67% of all energy used in direct energy production in the United States[16] alone, refractory nanophotonics can change the landscape of future energy technology. In particular, refractory nanophotonic devices with huge photonic density of states (PDOS) show great potential for significantly enhancing the efficiency of thermophotovoltaic devices.[17−27] Although natural hyperbolic materials are better in terms of PDOS enhancement than artificial ones, the state-of-the-art refractory hyperbolic material choices suffer from narrow bandwidth and lack of short infrared operation. For example, thermally stable hexagonal boron nitride (h-BN) and silicon carbide can support hyperbolic dispersions, but only in narrow ranges in 6−12 μm spectral window.[27−31] Layered graphite possesses hyperbolic dispersions in either the ultraviolet range or the long infrared wavelength range (>10 μm). Cuprates and ruthenates[32] supporting broadband hyperbolic dispersions face nanofabrication challenges, and it is not clear whether or not these are refractory materials. Addressing the lack of good refractory hyperbolic materials, we demonstrate aligned films of single-wall carbon nanotubes (SWCNTs) as an ideal broadband natural hyperbolic refractory material platform for thermal radiation engineering across the mid-infrared.

SWCNTs are one-dimensional materials possessing unique properties and, hence, are promising for applications including nanoelectronics and optoelectronics.[33−35] In particular, the strong quantum confinement results in extremely anisotropic electronic, optical[36] and thermal properties,[37] making them

Received: March 24, 2019
Published: June 26, 2019

DOI: 10.1021/acsphotonics.9b00452
ACS Photonics 2019, 6, 1602−1609

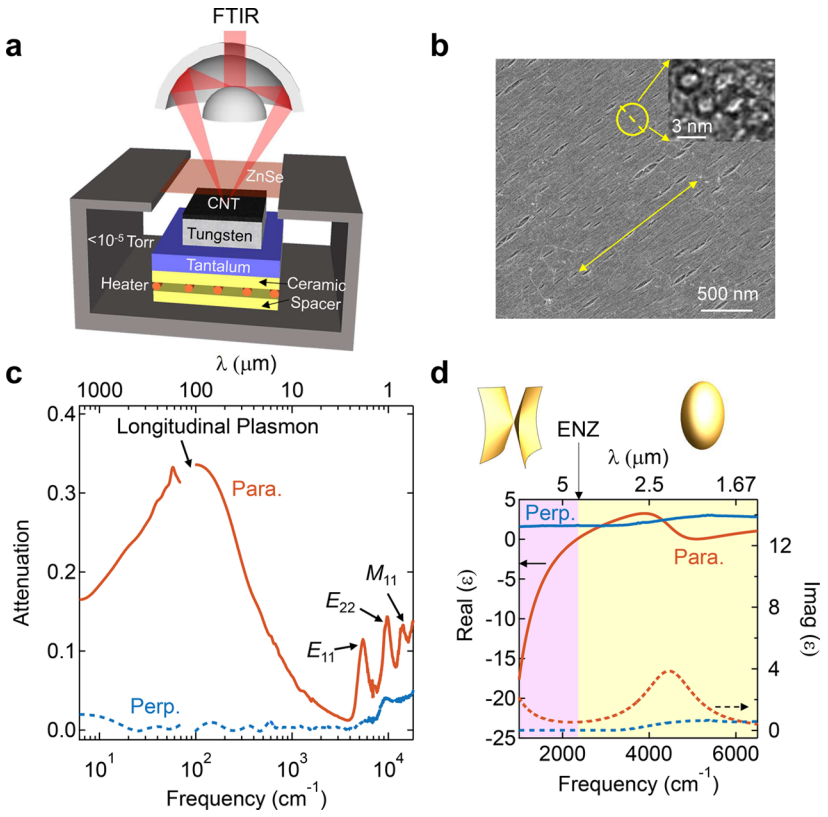

Figure 1. Fabrication and characterization of macroscopically aligned SWCNTs as a mid-infrared hyperbolic material. (a) Schematic diagram of the experimental setup for thermal emission and reflectivity measurements at temperatures up to 700 °C. Samples were heated using a PID-controlled resistive heater surrounded by ceramic spacers under high vacuum $<10^{-5}$ Torr. A tantalum film was used to support samples and block the direct thermal emission from the heater. A zinc selenide (ZnSe) window provides optical access for the light collection and analysis using a microscope and a Fourier transform infrared (FTIR) spectrometer, respectively. (b) A scanning electron micrograph and a transmission electron micrograph (inset), demonstrating a perfect alignment and high packing density. (c) Polarization attenuation spectra in a wide frequency range, from the THz/far-infrared range to the visible range, at room temperature. (d) The dielectric constants parallel and perpendicular to the SWCNT alignment direction, with an ENZ frequency in the mid-infrared range.

exceptional for thermal radiation engineering. To preserve these extraordinary properties at nanoscale in large-scale device applications requires a fabrication technique of producing ensembles of SWCNTs with macroscopic alignment, high packing density, controllable metallicity and chirality, and compatibility with facile nano/micromanufacturing, but it had been a grand challenge of developing successful methods. Recently, we developed a versatile vacuum filtration technique to prepare such aligned SWCNT films,[38] paving the way for highly anisotropic thermal emitters.

A closely packed bundle of aligned metallic or doped semiconducting SWCNTs can be described as a uniaxial anisotropic medium with effective permittivities $\varepsilon_{\parallel}$ and $\varepsilon_{\perp}$ along the tube axis and in the perpendicular plane, respectively. The conductivity due to free carriers along the nanotubes causes a metallic optical response, leading to $\mathrm{Re}(\varepsilon_{\parallel}) < 0$. In contrast, the nanotubes are insulating in the perpendicular plane, leading to $\mathrm{Re}(\varepsilon_{\perp}) > 0$. This extreme anisotropy leads to a broadband hyperbolic dispersion, which spans a majority of the mid-infrared range, a significant portion of the spectrum of interest for selective thermal emitters. The enhancement of PDOS in hyperbolic materials is limited by the geometry of the material, that is, the validity limit of the effective medium approximation ($|k_{max} \cdot d| \ll 1$), which depends on the highest momentum photons supported by the system (k_{max}) and the characteristic periodicity (d).[21,22,39,40] However, because of the extremely small diameters of SWCNTs (~1 nm), highly aligned and densely packed SWCNT films can support much higher k modes, enabling over 1000× enhancement in PDOS. The combination of hyperbolic dispersion and ultrahigh chemical stability up to 1600 °C[41] make aligned SWCNTs a promising platform for mid-infrared refractory nanophotonics and thermal radiation engineering.[42]

Here, we report hyperbolic thermal emitters emitting spectrally selective and polarized mid-infrared radiation with a 700 °C operating temperature. This novel emitter is based on highly aligned and densely packed SWCNTs prepared through spontaneous alignment that occurs during vacuum filtration.[38] In comparison to vertically aligned SWCNTs grown by the chemical-vapor-deposition (CVD) method,[43] our films have a significantly higher packing density, sustain high temperatures, and are robust during nanofabrication. We demonstrate that aligned SWCNT films have a hyperbolic dispersion at wavelengths longer than 4.3 μm (<2335 cm^{-1}) at 700 °C. In direct thermal emission measurements, we observed strongly polarized and narrowband radiation from aligned SWCNT thin films originating from the Berreman modes excited near the epsilon-near-zero (ENZ) frequency. Furthermore, we demonstrate propagating high-k photons in the hyperbolic medium, enabling enhanced thermal emission in deep subwavelength cavities of volume ~$\lambda^3/700$, where λ is the resonance wavelength. The thermal emission is widely tunable in the

DOI: 10.1021/acsphotonics.9b00452
ACS Photonics 2019, 6, 1602−1609

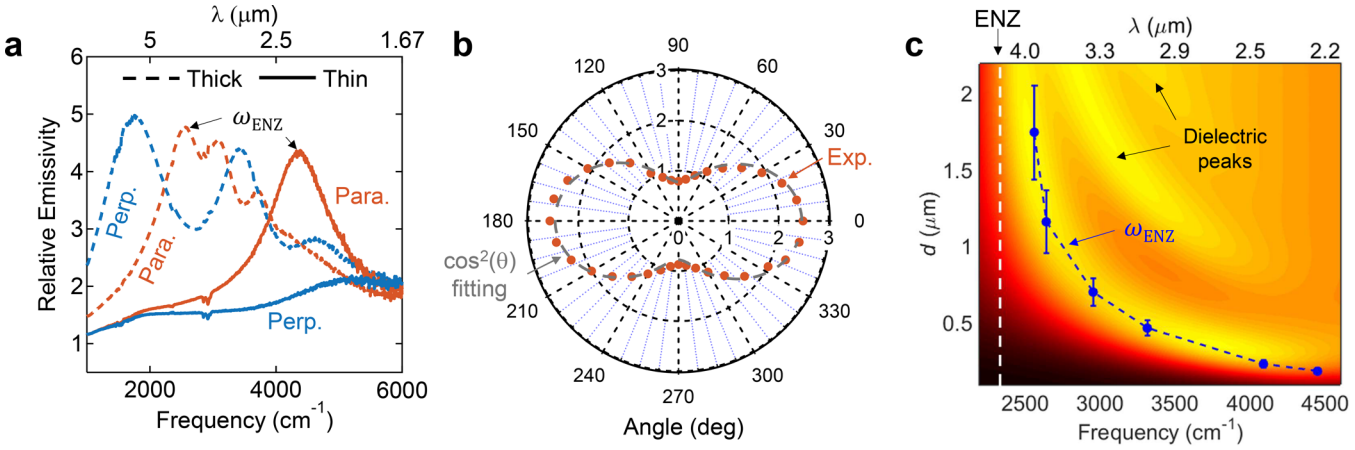

Figure 2. Thermal emission from continuous films of aligned SWCNTs. (a) Relative emissivity of a 188 nm thick film and a 1.75 μm thick film on tungsten substrates, parallel and perpendicular to the SWCNT alignment direction, respectively. The measurement was performed at 700 °C. The emission spectra were normalized to the spectrum from a bare tungsten substrate with the emissivity spectrum shown in Figure S4b. (b) Polarization-dependent integrated emission signal over frequency for the 188 nm thick film in polar coordinates. A $\cos^2(\theta)$ fitting matches the experimental data well. (c) The calculated emission spectra for various film thicknesses d. The experimental peak position of ω_{ENZ} is overlay as the blue dots connected by a dashed line. A clear asymptomatic approach as thickness increases is observed. As film thickness increases, dielectric peaks also emerge.

mid-infrared range by adjusting the dimensions of the aligned SWCNT structures.

In order to demonstrate unique optical and thermal radiation properties of the aligned SWCNT structures, we measured their thermal emission and reflectivity at temperatures up to 700 °C using a Fourier transform infrared (FTIR) spectrometer, equipped with a reflective microscope and a heated vacuum stage (see Figure 1a). See Materials and Methods for more details of the experimental setup. Macroscopically aligned, densely packed SWCNT films were prepared by filtrating a well-dispersed SWCNT suspension through a 2 in. filtration system.[38,44] The as-prepared films contained both metallic and semiconducting nanotubes with an average diameter of 1.4 nm. The obtained films were well aligned and densely packed, as observed in the scanning electron micrograph of Figure 1b and the cross-sectional transmission electron micrograph in the inset of Figure 1b. The SWCNT films were transferred onto different substrates using a standard wet transfer technique.[38] We further fabricated indefinite cavities using electron beam lithography and reactive ion etching. See Materials and Methods and Supporting Information, Figure S1, for the details of the wet transfer and nanofabrication processes and additional sample characterization data.

A room-temperature optical absorption spectrum for a densely packed aligned SWCNT film in a broad spectral range is shown in Figure 1c, from terahertz (THz) to visible, obtained using THz time-domain spectroscopy, FTIR, and visible-near-IR spectroscopy. The optical absorption is strongly polarization dependent. When the polarization is perpendicular to the tube axis, the absorption is small and featureless. On the other hand, a prominent absorption peak at ~100 cm^{-1} is observed for the parallel polarization case arising from the longitudinal plasmon resonance[45] in finite-length SWCNTs. Further, absorption peaks in the near-infrared and visible ranges, arising from the first two interband transitions for semiconducting tubes (E_{11} and E_{22}) and the first interband transition for metallic tubes (M_{11}) are clearly observed in the parallel polarization case.

Wavelength-dependent dielectric constants of the SWCNT films in both directions ($\varepsilon_{\parallel}$ and $\varepsilon_{\perp}$) were extracted from reflectance measurements at room temperature and 700 °C. The aligned SWCNT film was treated as anisotropic bulk optical medium using effective medium theory. This effective medium accounted for disorder in the film and included the contributions from both metallic and semiconducting nanotubes. A combination of Drude and Lorentz oscillators[45] were used to retrieve the dielectric function in the parallel direction, and a point-wise retrieval[46] was employed for the perpendicular case. The robustness of the Drude-Lorentz model was verified by another retrieval technique based on Kramers–Kronig transformation; see Supporting Information, Note 1 and Figure S2. When the incident light polarization is perpendicular to alignment direction, SWCNTs are weakly absorbing because of geometry-induced depolarization effect. Thus, their imaginary permittivity in the perpendicular direction was assumed negligible at various temperatures; see Supporting Information, Note 1, for more details. At room temperature, the aligned SWCNT film have a hyperbolic dispersion below 3300 cm^{-1} (>3 μm). The room temperature dielectric constants are reported in the Supporting Information, Figure S3c. At 700 °C, the extracted dielectric functions are very similar to the room temperature measurements except for increased Drude damping and a slight red-shift in the plasma frequency at 700 °C. The red-shift in the plasma frequency can be attributed to high-temperature-induced dedoping.[47] However, the optical properties of aligned SWCNTs remained stable under vacuum after dedoping during the first heating cycle. Reflectivity measurements during heating cycles are discussed in Supporting Information, Note 1 and Figure S3.

Figure 1d shows the real and imaginary parts of the extracted ordinary and extraordinary dielectric constants in both directions at 700 °C. The permittivity perpendicular to the tube axis shows a low-loss dielectric behavior over the whole spectral range ($\mathrm{Re}(\varepsilon_{\perp}) > 0$, $\mathrm{Im}(\varepsilon_{\perp}) \approx 0$), whereas the permittivity parallel to the tube axis is metallic ($\mathrm{Re}(\varepsilon_{\parallel})$) in the mid-infrared with an ENZ frequency of about 2335 cm^{-1} (4.3

DOI: 10.1021/acsphotonics.9b00452
ACS Photonics 2019, 6, 1602−1609

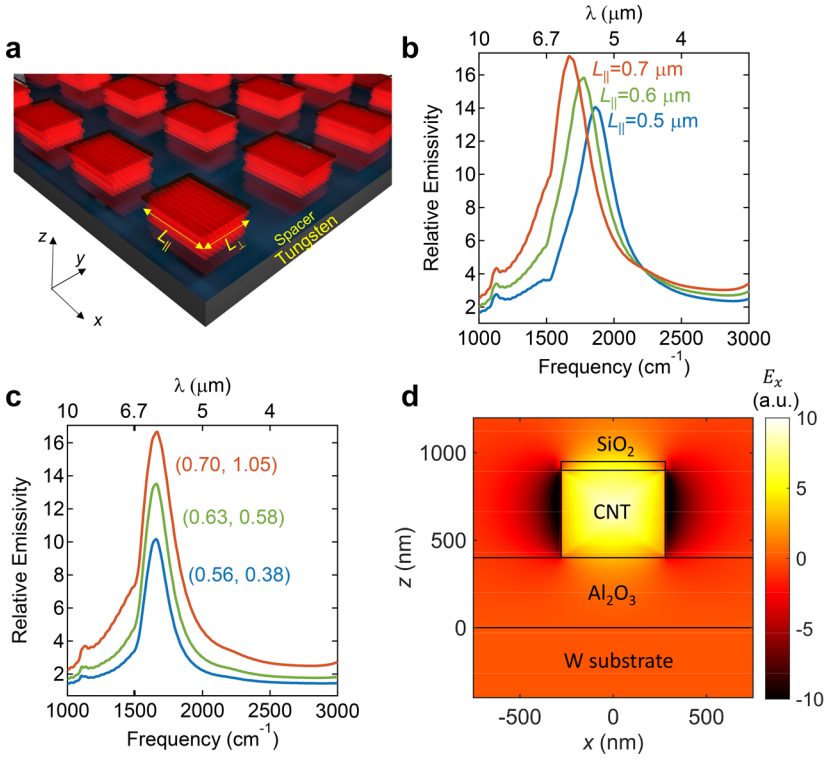

Figure 3. FDTD simulations on an array of SWCNT indefinite cavities. (a) Schematic diagram of a square lattice of indefinite cavities optimized for selective thermal emission. A spacer is included to suppress the plasmonic interaction with metallic substrates. The dimension along (perpendicular to) the tube axis is $L_{\parallel}$ ($L_{\perp}$), and the film thickness is d. All quantities are in μm. (b) FDTD calculations of relative emissivity for three cavities with tunable $L_{\parallel}$ and fixed $L_{\perp}$ = 1.05 μm. (c) FDTD calculations of relative emissivity for three cavities tuned along the isofrequency contour. (d) The electric field (E_x) profile of the (0.56, 0.38) cavity at the peak emissivity.

μm). While the real permittivities have different signs in different directions for frequencies smaller than the ENZ frequency, they are both positive for higher frequencies. The extreme anisotropy for frequencies smaller than the ENZ frequency results in a hyperbolic dispersion or hyperboloid isofrequency surface, an open surface with an unbounded surface area. The aligned SWCNT film supports a hyperbolic dispersion below 2335 cm^{-1} (>4.3 μm) at 700 °C, covering a significant portion of the region of interest for selective thermal emitters.

To demonstrate the hyperbolic behavior of aligned SWCNT films, we first characterized the thermal emission from continuous films. The frequency at which the dispersion goes from ellipsoidal to hyperbolic is the ENZ frequency (ω_{ENZ}), where we would expect the maximum thermal emission from continuous, thin films.[21] The ω_{ENZ} peak originates from the impedance matching condition in the multilayer structure, leading to the excitation of Berreman modes.[48] Thermal emission measurements of continuous, planar films of aligned SWCNTs on tungsten substrates at 700 °C are shown in Figure 2. Figure 2a shows polarization-dependent thermal emission from two different SWCNT films with thicknesses of 188 nm and 1.75 μm, respectively. All emission spectra are normalized with respect to the emission spectrum of the bare reference tungsten substrate with the emissivity spectrum shown in Figure S4b. In the case of the thinner film (188 nm), we clearly observe a prominent emission peak denoted as ω_{ENZ} in the parallel polarization, whereas no such peak is observed in the perpendicular polarization. Since there is no ENZ point in the perpendicular polarization, we do not see any enhanced thermal emission. The polarization dependence of the thermal emission from the 188 nm thick film is shown in Figure 2b. The experimental data can be fit with a $\cos^2\theta$ curve very well, which is also consistent with the polarization-dependent absorptivity in aligned SWCNTs.[49] A contrast over three in emission intensity is observed between the two orthogonal polarizations.

Figure 2c shows calculated emission spectra for various film thicknesses based on the transfer matrix method (hot colormap mapping) and the ω_{ENZ} peak seen in experiments (blue dots connected by a dashed line). As the SWCNT film thickness increases, ω_{ENZ} red-shifts to asymptotically approach the ENZ frequency. Thicker films also support Fabry−Pérot resonances, leading to several dielectric peaks in both parallel and perpendicular polarizations, as seen in Figures 2a,c. Thicker samples were fabricated via a manual stacking technique developed recently (see Materials and Methods for more details).[44] The experimental ω_{ENZ} peak matches well with calculations. We clearly observe that ω_{ENZ} approaches the ENZ frequency (white dashed line) when the film thickness increases, as shown in Figure 2c. The increasing error bars for thicker films are from the cumulative thickness uncertainty in the transfer process. Note that the influence of fabrication imperfections, including imperfect conformal transfer and small misalignment between layers, is expected to be negligible on thermal emission because the standard deviation in the angle of alignment of SWCNT films was found out to be less than 2°.[38] The stacking technique can indeed preserve alignment between layers very well and stack films consistently.[44]

Extremely large PDOS for hyperbolic materials implies that the medium can support a significantly larger number of

DOI: 10.1021/acsphotonics.9b00452
ACS Photonics 2019, 6, 1602−1609

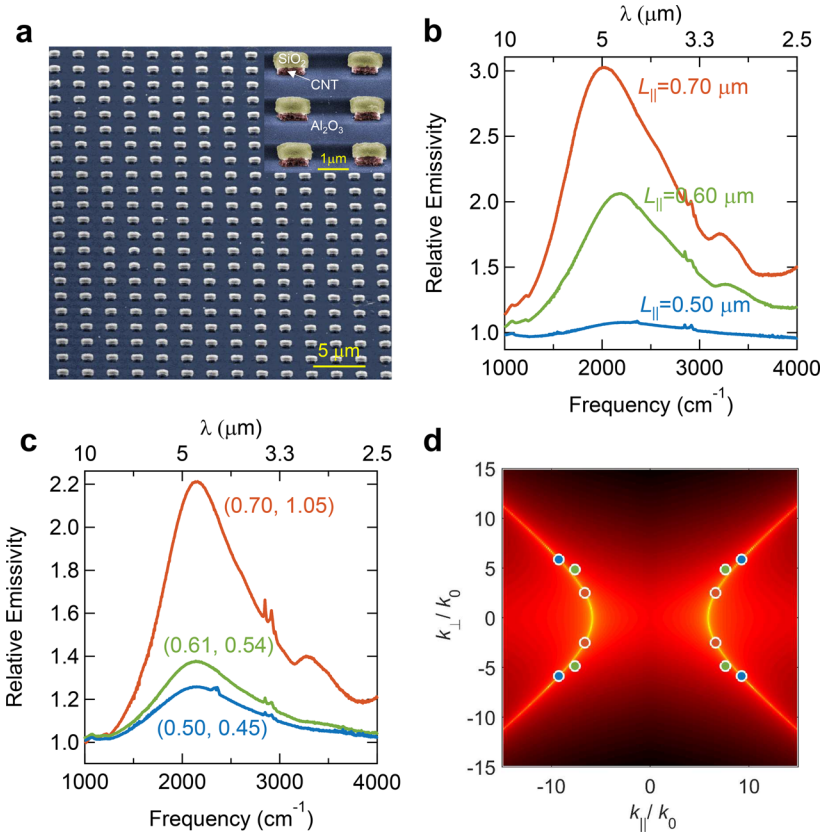

Figure 4. Thermal emission from SWCNT indefinite cavities. (a) Representative false-color scanning electron micrographs of fabricated SWCNT indefinite cavities. The inset describes a detailed structure of fabricated cavities. (b) Experimentally measured relative emissivity for three cavities with tunable $L_{\parallel}$ and fixed $L_{\perp}$ = 1.5 μm. The emission spectra were normalized to the spectrum from a bare tungsten substrate with the emissivity spectrum shown in Figure S4b. (c) Experimentally measured relative emissivity of three cavities with different combinations of dimensions in μm. All cavities show the same emission peak position at 2140 cm^{-1} (4.7 μm). (d) The extracted hyperbolic dispersion based on the dielectric constants at 2140 cm^{-1} from Figure 1d. $k_{\parallel}$ is the wavevector component along the tube alignment direction (x-axis), $k_{\perp}$ is that perpendicular to the alignment direction in the film plane (y-axis), and k_0 is the wavevector in vacuum.

thermal photons per unit volume than a blackbody. In other words, a hyperbolic medium can support the same number of thermal photons as a blackbody in a much smaller volume. However, not all of these thermal photons radiate out to far-field because of momentum mismatch. Nanostructuring hyperbolic materials can resonantly outcouple some of these photons and provide information about their momentum. Thus, observing resonances in far-field thermal emission from subwavelength cavities of hyperbolic or indefinite materials allows probing the momentum of high-k thermal photons supported by the medium.[50,51] By experimentally measuring the momentum of high-k thermal photons, a lower bound on k_{max} can be determined. From this lower bound, the PDOS can be determined through $\rho(\omega) \approx k_{max}^3$.[52] Figure 3 summarizes finite-difference-time-domain (FDTD) simulation results of SWCNT indefinite cavities. We considered a square lattice of SWCNT indefinite cavities on a tungsten substrate with a 400 nm thick Al_2O_3 spacer, as shown in the schematic of Figure 3a. The 400 nm thick Al_2O_3 spacer reduces any plasmonic interaction between the cavities and the tungsten substrate. We included a 50 nm thick SiO_2 layer on top of SWCNTs, which served as an etch mask during fabrication. The array period and the thickness of the SWCNT layer were fixed at 2.5 μm and 500 nm, respectively. The lengths of the cavity in directions parallel and perpendicular to the tube axis are denoted by $L_{\parallel}$ and $L_{\perp}$, respectively. Invoking Kirchoff's law, we calculated the emissivity spectra for various $L_{\parallel}$ and $L_{\perp}$ combinations. Figure 3b shows the calculated emissivity relative to the tungsten substrate as a function of frequency for indefinite cavities with various $L_{\parallel}$ and constant $L_{\perp}$ at 1.05 μm. An emissivity peak is observed only in the polarization parallel to the tube axis and originates from the hyperbolic resonance in the deep subwavelength cavities. The resonance red-shifts with increasing $L_{\parallel}$, as expected in any plasmonic or photonic structures.

However, indefinite cavities differ from conventional plasmonic or photonic cavities in that their resonance scales anomalously with $L_{\parallel}$ and $L_{\perp}$,[50,51] as demonstrated in Figure 3c. Here, we designed three cavities with different combinations of $L_{\parallel}$ and $L_{\perp}$ in such a way that the emissivity peak occurs at the same frequency. The dimensions of the three cavities chosen in Figure 3c are indicated in the parentheses as ($L_{\parallel}$, $L_{\perp}$) in μm. Note that $L_{\parallel}$ and $L_{\perp}$ scale the same way, unlike in conventional cavities, to keep the resonance at the same position. Also, all of these cavities are deeply subwavelength and support the same TM_{11} resonance. Figure 3d shows the resonant electric field (E_x) distribution for the smallest cavity (see Supporting Information, Figure S5, for more data). Unlike plasmonic resonators, the field inside an indefinite cavity is enhanced, similar to a photonic resonance. Since the optical losses that lead to thermal radiation are present primarily inside the cavity, the field enhancement effectively leads to enhanced thermal

DOI: 10.1021/acsphotonics.9b00452
ACS Photonics 2019, 6, 1602−1609

radiation. The divergence of the Poynting vector presented in Figure S5a–c shows the location where thermal emission originates.

We fabricated an array of indefinite cavities; false-color scanning electron micrographs are shown in Figure 4a. The inset shows the SiO_2 mask, 500 nm thick patterned CNT cavities, and the 400 nm thick Al_2O_3 film on the tungsten substrate. Figure 4b shows measured relative thermal emission spectra from indefinite cavities with a fixed $L_\perp$ of 1.5 μm and three different values of $L_\parallel$. The emissivity peaks red-shift with increasing $L_\parallel$, in qualitative agreement with the simulations results shown in Figure 3b. Increasing $L_\perp$ while fixing $L_\parallel$ results in a blue-shift; see Supporting Information, Note 3 and Figure S6.

By simultaneously changing $L_\perp$ and $L_\parallel$, we can maintain the resonance frequency at a single frequency, as shown in Figure 4c. For all three different ($L_\parallel$, $L_\perp$) combinations, the cavities emit resonantly at 2140 cm^{-1} (4.7 μm). This emission peak is slightly blue-shifted from the simulations and is also broader largely due to fabrication imperfections. By tuning the dimensions of the cavities so that the resonances trace an isofrequency contour, the dispersion of the SWCNT layer can be determined at this frequency. Figure 4d plots the experimentally measured dispersion points on the isofrequency contour of the SWCNT film calculated from the previously measured dielectric constants of the SWCNT film at 2140 cm^{-1}. Here, $k_\parallel$ is the wavevector component along the tube alignment direction (x-axis), $k_\perp$ is that perpendicular to the alignment direction in the film plane (y-axis), and k_0 is the wavenumber in vacuum. The measured dispersion agrees well with the calculations, confirming the existence of a hyperbolic dispersion behind the observed thermal emission behaviors. Further, the observation of resonances in deep subwavelength sized cavities proves that high-k waves supported in the SWCNT hyperbolic medium lead to significantly high PDOS or density of thermal photons. The smallest cavity in which we observed a resonance had a volume of $\sim\lambda^3/700$, corresponding with at least a 100× enhancement of PDOS in SWCNT hyperbolic thermal emitters.

We demonstrated that aligned SWCNTs make an excellent material platform for refractory nanophotonics in the mid-infrared. Our aligned SWCNT devices showed broadly tunable, polarized, and spectrally selective hyperbolic thermal emitters operating at 700 °C. While thin films of aligned SWCNTs exhibited enhanced thermal emission near their ENZ frequency due to the excitation of Berreman modes, nanopatterned films showed geometry-tunable spectrally selective thermal emission arising from indefinite cavity resonances. These resonances in deep subwavelength cavities allowed direct measurements of hyperbolic dispersions in SWCNT films, proving the existence of propagating high-k waves and significantly large PDOS. Photonic-like resonances in cavities of volume as small as $\lambda^3/700$ showed that the density of thermal photons in the SWCNT hyperbolic medium is greater than that in a blackbody by at least 100×.

METHODS

Thermal Emission and Reflectivity Experimental Setup. A Thermo Fisher Scientific Fourier transform infrared (FTIR) spectrometer, equipped with a microscope and a customized high-vacuum PID-controlled heating element, was used to measure the thermal emission and reflectivity of aligned SWCNT structures. The microscope has a reflective infrared objective, with NA = 0.24 (corresponding to a collection angle ∼14°) and aperture size 300 μm × 300 μm. A zinc selenide (ZnSe) window with antireflection coating was mounted on the heating stage for the light collection in the whole mid-infrared region, from 1000 to 7000 cm^{-1}. The heating element consists of a resistive heater surrounded by ceramic spacers. A tantalum film was used to support samples and block the direct thermal emission from the heater. The heating element was kept at target temperatures for at least 30 min to reach thermal equilibrium before any measurements. All experiments were performed under high vacuum $<10^{-5}$ Torr. Absolute emissivity calibration was performed by measuring thermal emission from a reference tungsten substrate. The high temperature emission spectrum of tungsten was determined through high temperature reflectance measurements shown in Figure S4a.

SWNCT Sample Preparation and Indefinite Cavity Fabrication. Arc-discharge P2-SWCNTs with an average diameter 1.4 nm were purchased from Carbon Solutions, Inc. A total of 20 mL of 0.5% (wt/vol) sodium deoxycholate (DOC, Sigma-Aldrich) was used to disperse 8 mg P2-SWCNTs. A tip sonicator was used to homogenize the suspension for 45 min, and the obtained suspension was ultracentrifuged for 1.5 h at 38000 rpm to remove undispersed large bundles and impurities. Well-dispersed supernatant was collected, and then diluted to reduce the surfactant concentration below the critical michelle concentration (CMC) of DOC, which is considered to be a necessary condition for spontaneous alignment. The diluted suspension was then poured into a 2 in. vacuum filtration system to have a uniform, aligned, and densely packed SWCNT film. The obtained film can be transferred to various substrates, by dissolving the filter membrane in chloroform and then rinsing the sample in acetone.[38] Furthermore, multiple thin aligned films were stacked to have a thicker film by manually transferring several pieces onto the substrate one by one, while preserving the alignment direction.[44]

A 400 nm thick film of Al_2O_3 was deposited onto a tungsten substrate in an reaction of trimethylaluminum and water using an atomic layer deposition system. A thick film of aligned SWCNTs was transferred onto the Al_2O_3 film using the aforementioned stacking process. A 50 nm thick film of SiO_2 was deposited onto the stacked SWCNT film as a hard mask, using an ultrahigh vacuum DC sputtering system. This hard mask aims to increase the dry etching selectivity for SWCNT patterning. We used standard electron beam lithography to define large-area patterns. A SU-8 positive lithography resist was deposited, following the coating of a thin layer of Omnicoat for easy lift-off. The patterns were first transferred onto the SiO_2 hard mask using a sulfur hexafluoride (SF_6) based reactive ion etching (RIE), and the SU-8 resist was removed using PG remover. Finally, a pure oxygen RIE was performed to transfer the patterns onto SWCNTs to form indefinite cavities.

ASSOCIATED CONTENT

Supporting Information

The Supporting Information is available free of charge on the ACS Publications website at DOI: 10.1021/acsphotonics.9b00452.

AFM characterization, optical constant recovery method, thermal stability measurements, additional field profiles,

DOI: 10.1021/acsphotonics.9b00452
ACS Photonics 2019, 6, 1602–1609

and experimental measurements of indefinite cavity tuning (PDF)

AUTHOR INFORMATION

Corresponding Author

*E-mail: guru@rice.edu.

ORCID

Junichiro Kono: 0000-0002-4195-0577

Gururaj V. Naik: 0000-0002-3800-3392

Author Contributions

[§]These authors contributed equally to this work (W.G. and C.F.D.).

Funding

U.S. Department of Energy Basic Energy Science Program DE-FG02-06ER46308, U.S. National Science Foundation ECCS-1708315, and Robert A. Welch Foundation C-1509

Notes

The authors declare no competing financial interest.

ACKNOWLEDGMENTS

W.G., X.L., and J.K. acknowledge support by the Basic Energy Science (BES) program of the U.S. Department of Energy through Grant No. DE-FG02-06ER46308 (for preparation of aligned carbon nanotube films), the U.S. National Science Foundation through Grant No. ECCS-1708315 (for optical measurements), and the Robert A. Welch Foundation through Grant No. C-1509 (for structural characterization measurements).

REFERENCES

(1) Greffet, J.-J.; Carminati, R.; Joulain, K.; Mulet, J.-P.; Mainguy, S.; Chen, Y. Coherent emission of light by thermal sources. *Nature* **2002**, *416*, 61−64.

(2) Schuller, J. A.; Taubner, T.; Brongersma, M. L. Optical antenna thermal emitters. *Nat. Photonics* **2009**, *3*, 658.

(3) Liu, X.; Tyler, T.; Starr, T.; Starr, A. F.; Jokerst, N. M.; Padilla, W. J. Taming the blackbody with infrared metamaterials as selective thermal emitters. *Phys. Rev. Lett.* **2011**, *107*, 045901.

(4) Liu, J.; Guler, U.; Lagutchev, A.; Kildishev, A.; Malis, O.; Boltasseva, A.; Shalaev, V. M. Quasi-coherent thermal emitter based on refractory plasmonic materials. *Opt. Mater. Express* **2015**, *5*, 2721−2728.

(5) Costantini, D.; Lefebvre, A.; Coutrot, A.-L.; Moldovan-Doyen, I.; Hugonin, J.-P.; Boutami, S.; Marquier, F.; Benisty, H.; Greffet, J.-J. Plasmonic metasurface for directional and frequency-selective thermal emission. *Phys. Rev. Appl.* **2015**, *4*, 014023.

(6) Dyachenko, P.; Molesky, S.; Petrov, A. Y.; Störmer, M.; Krekeler, T.; Lang, S.; Ritter, M.; Jacob, Z.; Eich, M. Controlling thermal emission with refractory epsilon-near-zero metamaterials via topological transitions. *Nat. Commun.* **2016**, *7*, na.

(7) Ilic, O.; Bermel, P.; Chen, G.; Joannopoulos, J. D.; Celanovic, I.; Soljačić, M. Tailoring high-temperature radiation and the resurrection of the incandescent source. *Nat. Nanotechnol.* **2016**, *11*, 320−324.

(8) Challener, W.; Peng, C.; Itagi, A.; Karns, D.; Peng, W.; Peng, Y.; Yang, X.; Zhu, X.; Gokemeijer, N.; Hsia, Y.-T.; et al. Heat-assisted magnetic recording by a near-field transducer with efficient optical energy transfer. *Nat. Photonics* **2009**, *3*, 220.

(9) Stipe, B. C.; Strand, T. C.; Poon, C. C.; Balamane, H.; Boone, T. D.; Katine, J. A.; Li, J.-L.; Rawat, V.; Nemoto, H.; Hirotsune, A.; et al. Magnetic recording at 1.5 Pb m- 2 using an integrated plasmonic antenna. *Nat. Photonics* **2010**, *4*, 484.

(10) Inoue, T.; De Zoysa, M.; Asano, T.; Noda, S. Filter-free nondispersive infrared sensing using narrow-bandwidth mid-infrared thermal emitters. *Appl. Phys. Express* **2014**, *7*, 012103.

(11) Lochbaum, A.; Fedoryshyn, Y.; Dorodnyy, A.; Koch, U.; Hafner, C.; Leuthold, J. On-chip narrowband thermal emitter for mid-IR optical gas sensing. *ACS Photonics* **2017**, *4*, 1371−1380.

(12) Coutts, T. J.; Fitzgerald, M. C. Thermophotovoltaics. *Sci. Am.* **1998**, *279*, 90−95.

(13) Basu, S.; Chen, Y.-B.; Zhang, Z. Microscale radiation in thermophotovoltaic devices—a review. *Int. J. Energy Res.* **2007**, *31*, 689−716.

(14) Kraemer, D.; Poudel, B.; Feng, H.-P.; Caylor, J. C.; Yu, B.; Yan, X.; Ma, Y.; Wang, X.; Wang, D.; Muto, A.; et al. High-performance flat-panel solar thermoelectric generators with high thermal concentration. *Nat. Mater.* **2011**, *10*, 532.

(15) Lenert, A.; Bierman, D. M.; Nam, Y.; Chan, W. R.; Celanović, I.; Soljačić, M.; Wang, E. N. A nanophotonic solar thermophotovoltaic device. *Nat. Nanotechnol.* **2014**, *9*, 126−130.

(16) Estimated U.S. Energy Consumption in 2017, Lawrence Livermore National Laboratory, 2017; Available at https://flowcharts.llnl.gov/commodities/energy.

(17) Fiorino, A.; Zhu, L.; Thompson, D.; Mittapally, R.; Reddy, P.; Meyhofer, E. Nanogap near-field thermophotovoltaics. *Nat. Nanotechnol.* **2018**, *13*, 806.

(18) Yu, Z.; Sergeant, N. P.; Skauli, T.; Zhang, G.; Wang, H.; Fan, S. Enhancing far-field thermal emission with thermal extraction. *Nat. Commun.* **2013**, *4*, 1730.

(19) Jacob, Z.; Smolyaninov, I. I.; Narimanov, E. E. Broadband Purcell effect: Radiative decay engineering with metamaterials. *Appl. Phys. Lett.* **2012**, *100*, 181105.

(20) Biehs, S.-A.; Tschikin, M.; Ben-Abdallah, P. Hyperbolic metamaterials as an analog of a blackbody in the near field. *Phys. Rev. Lett.* **2012**, *109*, 104301.

(21) Guo, Y.; Cortes, C. L.; Molesky, S.; Jacob, Z. Broadband super-Planckian thermal emission from hyperbolic metamaterials. *Appl. Phys. Lett.* **2012**, *101*, 131106.

(22) Guo, Y.; Jacob, Z. Thermal hyperbolic metamaterials. *Opt. Express* **2013**, *21*, 15014−15019.

(23) Liu, X.; Zhang, R.; Zhang, Z. Near-field thermal radiation between hyperbolic metamaterials: Graphite and carbon nanotubes. *Appl. Phys. Lett.* **2013**, *103*, 213102.

(24) Drachev, V. P.; Podolskiy, V. A.; Kildishev, A. V. Hyperbolic metamaterials: new physics behind a classical problem. *Opt. Express* **2013**, *21*, 15048−15064.

(25) Poddubny, A.; Iorsh, I.; Belov, P.; Kivshar, Y. Hyperbolic metamaterials. *Nat. Photonics* **2013**, *7*, 948−957.

(26) Zhao, B.; Guizal, B.; Zhang, Z. M.; Fan, S.; Antezza, M. Near-field heat transfer between graphene/hBN multilayers. *Phys. Rev. B: Condens. Matter Mater. Phys.* **2017**, *95*, 245437.

(27) Shekhar, P.; Atkinson, J.; Jacob, Z. Hyperbolic metamaterials: fundamentals and applications. *Nano Convergence* **2014**, *1*, 14.

(28) Caldwell, J. D.; Kretinin, A. V.; Chen, Y.; Giannini, V.; Fogler, M. M.; Francescato, Y.; Ellis, C. T.; Tischler, J. G.; Woods, C. R.; Giles, A. J.; et al. Sub-diffractional volume-confined polaritons in the natural hyperbolic material hexagonal boron nitride. *Nat. Commun.* **2014**, *5*, 5221.

(29) Dai, S.; Fei, Z.; Ma, Q.; Rodin, A.; Wagner, M.; McLeod, A.; Liu, M.; Gannett, W.; Regan, W.; Watanabe, K.; et al. Tunable phonon polaritons in atomically thin van der Waals crystals of boron nitride. *Science* **2014**, *343*, 1125−1129.

(30) Yoxall, E.; Schnell, M.; Nikitin, A. Y.; Txoperena, O.; Woessner, A.; Lundeberg, M. B.; Casanova, F.; Hueso, L. E.; Koppens, F. H.; Hillenbrand, R. Direct observation of ultraslow hyperbolic polariton propagation with negative phase velocity. *Nat. Photonics* **2015**, *9*, 674.

(31) Tamagnone, M.; Ambrosio, A.; Chaudhary, K.; Jauregui, L. A.; Kim, P.; Wilson, W. L.; Capasso, F. Ultra-confined mid-infrared resonant phonon polaritons in van der Waals nanostructures. *Sci. Adv.* **2018**, *4*, No. eaat7189.

(32) Sun, J.; Litchinitser, N. M.; Zhou, J. Indefinite by nature: from ultraviolet to terahertz. *ACS Photonics* **2014**, *1*, 293−303.

(33) Avouris, P.; Chen, Z.; Perebeinos, V. Carbon-Based Electronics. *Nat. Nanotechnol.* **2007**, *2*, 605−615.

DOI: 10.1021/acsphotonics.9b00452
ACS Photonics 2019, 6, 1602−1609

(34) Avouris, P.; Freitag, M.; Perebeinos, V. Carbon-Nanotube Photonics and Optoelectronics. *Nat. Photonics* **2008**, *2*, 341−350.
(35) Ho, P.-H.; Farmer, D. B.; Tulevski, G. S.; Han, S.-J.; Bishop, D. M.; Gignac, L. M.; Bucchignano, J.; Avouris, P.; Falk, A. L. Intrinsically ultrastrong Plasmon−exciton interactions in crystallized films of carbon nanotubes. *Proc. Natl. Acad. Sci. U. S. A.* **2018**, *115*, 12662−12667.
(36) Chiu, K. C.; Falk, A. L.; Ho, P. H.; Farmer, D. B.; Tulevski, G.; Lee, Y. H.; Avouris, P.; Han, S. J. Strong and Broadly Tunable Plasmon Resonances in Thick Films of Aligned Carbon Nanotubes. *Nano Lett.* **2017**, *17*, 5641−5645.
(37) Dresselhaus, M. S., Dresselhaus, G., Avouris, P., Eds. *Carbon Nanotubes: Synthesis, Structure, Properties, and Applications*; Topics in Applied Physics 18; Springer: Berlin, 2001.
(38) He, X.; Gao, W.; Xie, L.; Li, B.; Zhang, Q.; Lei, S.; Robinson, J. M.; Hároz, E. H.; Doorn, S. K.; Wang, W.; Vajtai, R.; Ajayan, P. M.; Adams, W. W.; Hauge, R. H.; Kono, J. Wafer-Scale Monodomain Films of Spontaneously Aligned Single-Walled Carbon Nanotubes. *Nat. Nanotechnol.* **2016**, *11*, 633−638.
(39) Elser, J.; Wangberg, R.; Podolskiy, V. A.; Narimanov, E. E. Nanowire metamaterials with extreme optical anisotropy. *Appl. Phys. Lett.* **2006**, *89*, 261102.
(40) Elser, J.; Podolskiy, V. A.; Salakhutdinov, I.; Avrutsky, I. Nonlocal effects in effective-medium response of nanolayered metamaterials. *Appl. Phys. Lett.* **2007**, *90*, 191109.
(41) Yudasaka, M.; Kataura, H.; Ichihashi, T.; Qin, L.-C.; Kar, S.; Iijima, S. Diameter enlargement of HiPco single-wall carbon nanotubes by heat treatment. *Nano Lett.* **2001**, *1*, 487−489.
(42) Molesky, S.; Jacob, Z. Ideal near-field thermophotovoltaic cells. *Phys. Rev. B: Condens. Matter Mater. Phys.* **2015**, *91*, 205435.
(43) Murakami, Y.; Chiashi, S.; Miyauchi, Y.; Hu, M.; Ogura, M.; Okubo, T.; Maruyama, S. Growth of vertically aligned single-walled carbon nanotube films on quartz substrates and their optical anisotropy. *Chem. Phys. Lett.* **2004**, *385*, 298−303.
(44) Komatsu, N.; Gao, W.; Chen, P.; Guo, C.; Babakhani, A.; Kono, J. Modulation-Doped Multiple Quantum Wells of Aligned Single-Wall Carbon Nanotubes. *Adv. Funct. Mater.* **2017**, *27*, 1606022.
(45) Zhang, Q.; Hároz, E. H.; Jin, Z.; Ren, L.; Wang, X.; Arvidson, R. S.; Lüttge, A.; Kono, J. Plasmonic Nature of the Terahertz Conductivity Peak in Single-Wall Carbon Nanotubes. *Nano Lett.* **2013**, *13*, 5991−5996.
(46) Denton, R.; Campbell, R.; Tomlin, S. The determination of the optical constants of thin films from measurements of reflectance and transmittance at normal incidence. *J. Phys. D: Appl. Phys.* **1972**, *5*, 852.
(47) Wu, Z.; Chen, Z.; Du, X.; Logan, J.; Sippel, J.; Nikolou, M.; Kamaras, K.; Reynolds, J. R.; Tanner, D. B.; Hebard, A. F.; Rinzler, A. G. Transparent, Conductive Nanotube Films. *Science* **2004**, *305*, 1273−1276.
(48) Harbecke, B.; Heinz, B.; Grosse, P. Optical properties of thin films and the Berreman effect. *Appl. Phys. A: Solids Surf.* **1985**, *38*, 263−267.
(49) Murakami, Y.; Einarsson, E.; Edamura, T.; Maruyama, S. Polarization dependence of the optical absorption of single-walled carbon nanotubes. *Phys. Rev. Lett.* **2005**, *94*, 087402.
(50) Yao, J.; Yang, X.; Yin, X.; Bartal, G.; Zhang, X. Three-dimensional nanometer-scale optical cavities of indefinite medium. *Proc. Natl. Acad. Sci. U. S. A.* **2011**, *108*, 11327−11331.
(51) Yang, X.; Yao, J.; Rho, J.; Yin, X.; Zhang, X. Experimental realization of three-dimensional indefinite cavities at the nanoscale with anomalous scaling laws. *Nat. Photonics* **2012**, *6*, 450−454.
(52) Jacob, Z.; Kim, J.-Y.; Naik, G. V.; Boltasseva, A.; Narimanov, E. E.; Shalaev, V. M. Engineering photonic density of states using metamaterials. *Appl. Phys. B: Lasers Opt.* **2010**, *100*, 215−218.

DOI: 10.1021/acsphotonics.9b00452
ACS Photonics 2019, 6, 1602−1609